Plasma Sources Sci. Technol. **9** (2000) 116–127. Printed in the UK PII: S0963-0252(00)11317-9

Characterization of transformer coupled oxygen plasmas by trace rare gases–optical emission spectroscopy and Langmuir probe analysis

N C M Fuller†‡, M V Malyshev†, V M Donnelly† and Irving P Herman‡

† Bell Laboratories, Lucent Technologies, Murray Hill, NJ 07974, USA
‡ Department of Applied Physics, Columbia Radiation Laboratory, Columbia University, New York, NY 10027, USA

Received 8 October 1999, in final form 18 January 2000

Abstract. Trace rare gases–optical emission spectroscopy (TRG–OES) and Langmuir probe analysis have been used to measure the electron temperature, T_e, in a high-density inductively (transformer) coupled (TCP) 10 mTorr oxygen plasma as a function of the 13.56 MHz radio frequency (rf) power. The oxygen atomic densities were estimated by O-atom optical emission (8446 Å), and rare gas actinometry (Ar, 7504 Å). In the H-(inductive)-mode, T_e increases from 2.6 to 3.4 eV for the low-energy electrons sampled by the Langmuir probe and from ∼3.5 to 6.0 eV for the high-energy electrons sensed by TRG–OES as the rf power is increased from 120 to 1046 W. In the E-(capacitive)-mode, below 50 W, T_e measured by TRG–OES increases with rf power from ∼4 eV at very low power (∼7 W) to ∼6.1 eV at 45 W. Between the highest E-mode power (∼50 W) and lowest H-mode power (∼120 W), the T_e measured by TRG–OES drops from 6.1 to 3.5 eV, while T_e derived from Langmuir probe measurements drops only slightly from 3.0 to 2.6 eV. In the H-mode, the electron energy distribution function (EEDF) is bi-Maxwellian from ∼120 to 1046 W. In the E-mode, the EEDF changes from nearly Maxwellian (possibly Druyvesteyn) at low rf powers (∼7 W) to bi-Maxwellian at the higher E-mode powers (∼45 W). O_2 dissociation is low (∼2%) at the maximum rf power density of 5.7 W cm^{-2} (1046 W), and this low value is attributed to the high rate of O-atom recombination on the mostly stainless-steel walls. A detailed accounting of the sources of O (8446 Å) emission revealed significant contributions from electron impact excitation from O(^{1}S) and dissociative excitation of O_2.

1. Introduction

Oxygen-containing plasmas are widely used for photoresist etching and stripping [1, 2]. In addition, O_2 is a major component in plasma processes that are being developed for the etching of organic, low-dielectric-constant (so-called low-κ) thin films [3, 4]. These materials are being explored as candidates for future use as interlayer dielectrics in higher-speed circuits [3, 5]. The etching mechanisms, rates, and etched profile shapes in oxygen etching plasmas depend on the relative fluxes of O, O_2, O^+ and O_2^+. The determination of the neutral species densities as a function of radio frequency (rf) power and pressure is, thus, essential in the understanding and optimization of the plasma etching processes for all of these micro-electronic materials. Additionally, accurate determination of the electron temperature is important for understanding the rates of dissociation and ionization of neutral species in these plasmas, and in assessing the mechanisms for differential charging, which may contribute to undesirable etched profile anomalies and electrical damage due to charge build-up and current flow [6–8].

Oxygen plasmas have been extensively characterized to determine densities of neutral and charged species, electron energy distribution functions (EEDFs) and plasma potentials [2, 9–21]. Most of these are studies of either parallel plate reactors, or high-density electron cyclotron resonance (ECR) plasmas. Less work has been reported for oxygen inductively-coupled plasmas (ICPs) [19–21].

This paper reports measurements and calculations of the densities of ground-state atomic and molecular oxygen and of the principal metastable species of atomic oxygen (^{1}D and ^{1}S), as well as electron temperatures (T_e), in an inductively-coupled oxygen plasma (transformer-coupled plasma, TCP) as a function of the applied rf power at a pressure of 10 mTorr. Optical emission actinometry [22], modelling, and mass balance were used to estimate the atomic and molecular oxygen and the metastable species densities using the 8446 Å O-atom emission lines from the 3p ^{3}P level. An extension of

0963-0252/00/020116+12$30.00

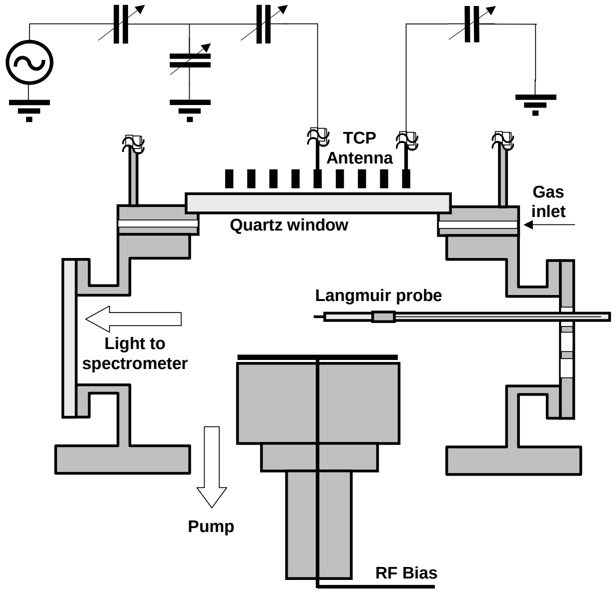

Figure 1. Schematic diagram of the TCP reactor, matching network and Langmuir probe.

this optical actinometry technique, trace rare gases optical emission spectroscopy (TRG–OES), was used to determine electron temperature T_e [23–30]. The electron temperature was also measured with a Langmuir probe, as were ion densities.

2. Experimental procedure

The reactor used in these experiments has been described previously and is shown in figure 1 [25, 30]. It consists of a stainless-steel cylindrical chamber of 36 cm inside diameter and 22 cm height. The chamber has a top port sealed by a 25 cm diameter quartz window. The TCP source includes a 6″ diameter, six-loop coil antenna and matching network (LAM Research) which are positioned above the top window. The RF power is delivered to the antenna by a 3 kW Plasma-Therm generator operating at 13.56 MHz. The He-gas-cooled chuck held a 5″ diameter silicon wafer that was rapidly oxidized to a presumed self-limiting thickness, such that continued exposure to the O_2 plasma during the experiment did not alter the composition of the substrate surface or in any way change the operation of the plasma. The TCP operates in a capacitively-coupled (dim or E) mode for powers below 60 W and in an inductively-coupled (bright or H) mode for powers above 100 W. The upper power limit of 1046 W corresponds to 5.7 W cm^{-2}, for the area defined by the antenna. For this study, no rf power was delivered to the stage, which was positioned 12 cm from the top quartz window. In all experiments, the pressure in the reactor was 10 mTorr, and the O_2 flow rate was 95 sccm.

The absolute species concentrations were measured by optical emission actinometry [22], with corrections for electron temperature dependences [27, 28]. Line-integrated plasma-induced emission from a region across the wafer and $\sim$2 cm above it was collected through a UV-grade quartz window on one side of the reactor. The emission was imaged through a long-pass coloured glass filter (to reduce signals from unwanted diffraction orders in the monochromator) onto the entrance slit of a 0.64 m focal length monochromator (ISA Incorporated, model no M64), equipped with a GaAs photomultiplier tube (PMT) (Hamamatsu model no R943-02). The monochromator was scanned from 4200 to 8950 Å at rates varying from 10 to 260 Å min^{-1} with a 0.80 Å bandpass. The emission intensities were corrected for the relative response of the monochromator and detector.

Electron temperatures (T_e^{OES}) were also measured by the TRG–OES technique that samples the high-energy tail of the EEDF (electron energies $\varepsilon > 10$ eV) [23–30]. In this measurement, a small amount (5 sccm = 5%) of a mixture containing equal volumes of He, Ar, Ne, Kr and Xe was added to the O_2 feed gas (95 sccm). The number density of each rare gas differed somewhat from the expected 1% of the total number density, owing to differences in the relative pumping speeds and transport efficiencies of the gases. These effects were taken into account [25] in the derivation of T_e^{OES} from a kinetic model that computes relative optical emission intensities and compares them to observed intensities, with the electron temperature as an adjustable parameter. The accuracy in T_e^{OES} was previously estimated to be about ±10% [25]. As shown below, the addition of rare gases caused no measurable change in the EEDFs measured with the Langmuir probe. In addition, the intensity of the O 8446 Å emission line was unaffected by the addition of the rare gases beyond simple dilution. Consequently, the addition of the rare gas mixture does not significantly perturb the properties of a pure oxygen discharge.

Positive ion densities (n_i^+) and electron temperatures (T_e^{LP}) were measured with a single, rf-compensated Langmuir probe (Scientific Systems Smart Probe). Full current–voltage (I–V) curves were recorded, spanning the range from ion saturation to electron saturation currents at voltages above the plasma potential. Because of the large area of grounded stainless-steel surfaces in contact with the plasma, a reasonably well defined plasma potential, V_{PP}, of 22 V could be determined, and, for bright-mode powers, high electron currents could be drawn to heat and thus clean the probe tip. Nonetheless, some fluctuations were observed in the raw voltages, which were correlated with ‘micro-discharges’ on the walls, presumably as a thin oxide layer breaks down and allows current to flow. A reference electrode supplied with the probe was used to correct for these probe-induced changes in the plasma potential at positive voltages.

In deriving T_e^{OES} and T_e^{LP} from optical emission measurements and Langmuir probe traces, a Maxwellian EEDF is assumed:

$$\frac{\mathrm{d}n}{\mathrm{d}\varepsilon} = \frac{2n_e}{\sqrt{\pi}} \frac{1}{(kT_e)^{3/2}} \sqrt{\varepsilon} \exp\left(\frac{-\varepsilon}{kT_e}\right). \tag{1}$$

T_e^{LP} was determined from I–V curves between $\sim$5 and 20 V (relative to the grounded reactor walls) and therefore represented the temperature of an assumed Maxwellian distribution between $\sim$2 and 17 eV (the plasma potential subtracting the above voltages). In addition, qualitative information on the EEDFs was derived from the I–V curves recorded at high powers, where the signal-to-noise ratio was sufficient to extend the electron energies to $\sim$22 eV. Full EEDFs were also obtained at the higher powers by finding

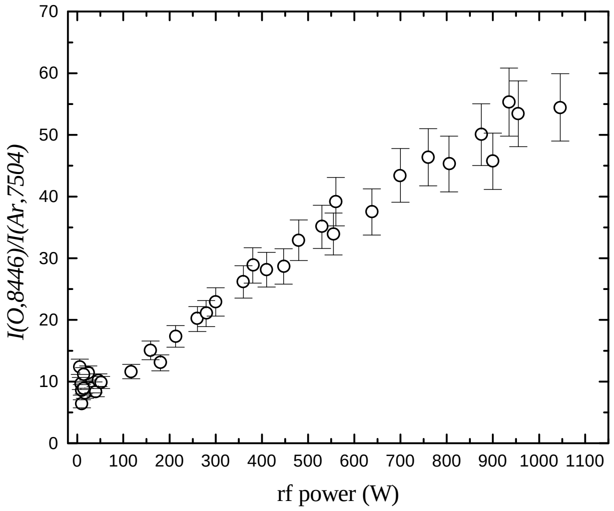

Figure 2. Ratio of the oxygen atom emission intensity at 8446 Å to that of argon at 7504 Å against rf power in a 10 mTorr O_2 TCP plasma with 5% of the trace rare gas mixture. The data have been corrected for the wavelength-dependent response of the spectrometer.

the second derivative of the current while dithering the probe voltage ±1 eV during data collection. The range of electron energies represented by T_e^{OES} is a complicated function of pressure and power. Typically, T_e^{OES} is the 'temperature' that best describes the electrons with energies higher than ~10 eV. Therefore, T_e^{OES} describes a higher-energy portion of the EEDF than does T_e^{LP}.

3. Results and discussions

3.1. Emission intensities and positive ion densities

Atomic emission intensities of O, Ar, Kr and Xe, were recorded from 7000 to 9000 Å as a function of rf power. Oxygen atom emission intensities at 8446 Å, corresponding to the $3p\,^3P \rightarrow 3s\,^3S^o$ transition, were normalized by the 7504 Å emission intensity from the Paschen $2p_1$ level of Ar. These actinometry ratios, corrected for changes in the spectrometer response, are presented in figure 2. They are used below to determine ground-state oxygen atom densities. The error bars on the data represent an estimated ±10% scatter in measurements performed under nominally identical conditions.

The Ar emission intensities I(Ar, 7504) used to derive the emission ratios in figure 2 are shown in figure 3. The mechanism for exciting the $2p_1$ level of Ar is one-step electron impact excitation from the ground state. Cross sections for this process were measured by Chilton *et al* [31]. The cross sections for excitation from the $1s_3$ and $1s_5$ Ar metastable levels to the $2p_1$ level are too small for these pathways to be important, given the low metastable number density [32]. Positive-ion densities measured with the Langmuir probe in the centre of the plasma 2.5 cm above the wafer are also included in figure 3. The positive-ion density reaches 1.0×10^{11} cm^{-3} at the highest power. I(Ar, 7504) in figure 3 is normalized to the positive-ion density at 1046 W. It increases more strongly with power than does n_i^+.

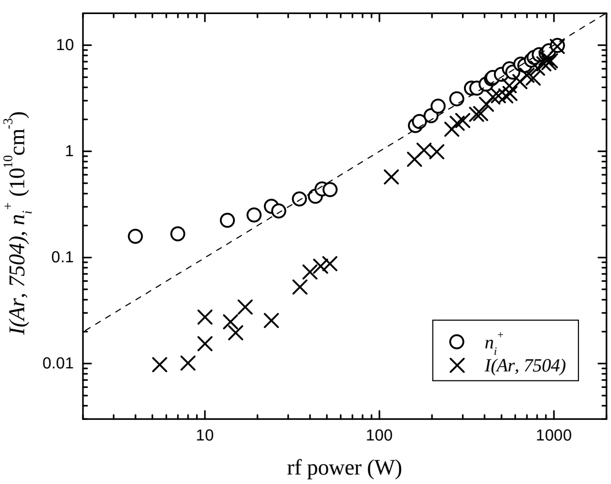

Figure 3. Positive-ion density (measured with a Langmuir probe) and the emission intensity of the Ar 7504 Å line against rf power in a 10 mTorr O_2 TCP plasma with 5% of the trace rare gas mixture. I(Ar, 7504) is normalized to n_i^+ at 1046 W; the broken line is the linear dependence.

This can be ascribed to an increase in T_e^{OES} with power (see below) and, possibly, also to a smaller fraction of negative ions relative to electrons at high power.

3.2. Electron temperature

Figure 4 shows a portion of a sample spectrum at 14 W rf power that includes several of the rare gas emission lines: Ar (7504, 7514 and 8115 Å), Kr (8104, 8113 and 8190 Å) and Xe (8231 Å). The intensities of these and other rare gas emission lines are used to determine electron temperature. In this TRG–OES method, optical emission intensities of Ar, Kr and Xe are computed from a model, and then compared to the experimentally measured intensities such as those shown in figure 4. The electron temperature is determined by the best match of the model to the observed relative emission intensities, with T_e^{OES} as the only adjustable parameter.

The electron temperatures measured by TRG–OES and Langmuir probe analysis, are presented in figure 5 as a function of discharge power. For the bright (inductive) mode power regime, T_e^{LP} increases from 2.6 to 3.4 eV when the power is increased from ~120 to 1046 W, whereas T_e^{OES} increases from ~3.5 to 6.0 eV over this power range. The primary cause of this difference can be attributed to the deviation of the EEDF from a pure Maxwellian form (see below) [20, 21, 33–42]. Further evidence for this behaviour is obtained from a closer examination of the I–V curves recorded in this power regime. Figure 6 presents a portion of five such curves, plotted as the natural logarithm of the electron current against voltage (V) for rf powers from 218 to 1046 W. From these typical curves, the T_e^{LP} obtained from the slopes between ~5 and 20 V (relative to ground) increases from 2.6 eV at 218 W to 3.4 eV at 1046 W. All T_e^{LP} values plotted in figure 5 were obtained from this low-voltage portion of these and other I–V curves. The increase in curvature in the plots in figure 6 as the rf power increases, indicates that in this power range, the high-energy electrons can be better described by a T_e that is 0.8 (745 W) to 1.8 eV

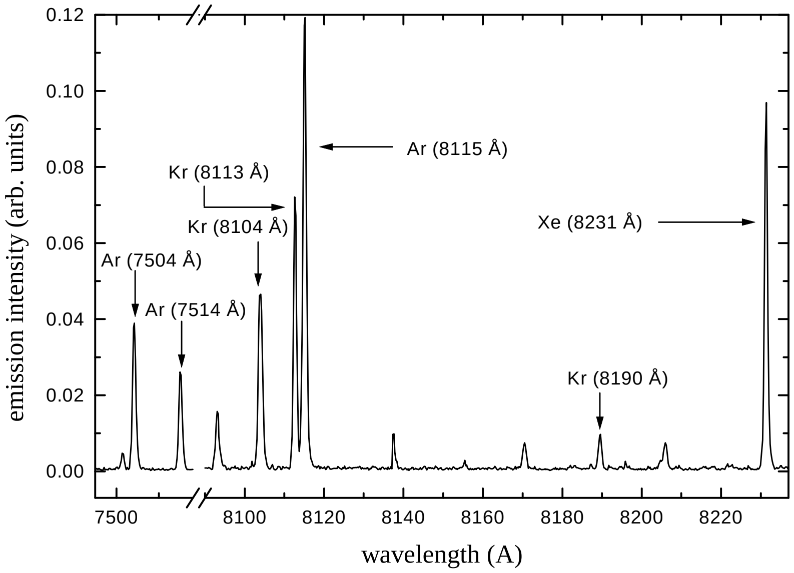

Figure 4. Optical emission spectrum from 7490 to 7516 Å and from 8090 to 8250 Å for a 10 mTorr O_2 TCP plasma at 14 W rf power with 5% of the trace rare gas mixture. The labelled rare gas emission lines are: Ar, 7504, 7514 and 8115 Å; Kr, 8104, 8113 and 8190 Å; and Xe, 8231 Å.

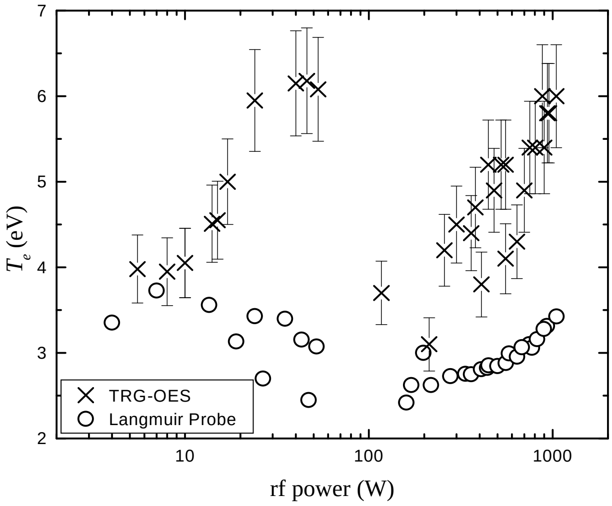

Figure 5. T_e against rf power in a 10 mTorr O_2 TCP plasma with 5% of the trace rare gas mixture measured by Langmuir probe and the TRG–OES method. The error bars on the T_e^{OES} values represent the estimated accuracy [25].

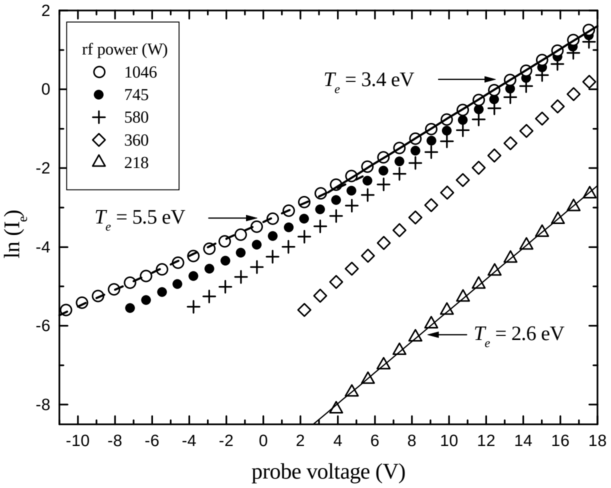

Figure 6. The ln (electron current) (that is, ln (total current measured by the Langmuir probe − positive-ion current)) against probe voltage at 218, 360, 580, 745 and 1046 W in a 10 mTorr O_2 TCP with 5% of the trace rare gas mixture.

(1046 W) higher than T_e^{LP}. This high-energy 'temperature', obtained from the slopes between −10 and ∼5 V, is very close to the T_e^{OES} value of ∼5.7 eV, measured in this power range for the high-energy part of the EEDF. Thus, in the H-mode (and in the E-mode as is discussed below), all of the differences between T_e^{LP} and T_e^{OES} can be explained by the deviation of the EEDF from a Maxwellian to a bi-Maxwellian form and the preferential sampling of the low- and high-energy regimes of the EEDF by the Langmuir probe and TRG–OES, respectively.

To further confirm the non-Maxwellian distribution of the electron energies, electron energy probability functions (EEPFs) were recorded at the higher powers; measurements at 980 W are presented in figure 7. The distributions have a noticeable bi-Maxwellian shape. Those at 980 W can be described by a T_e of 3.03 eV for the lower-energy electrons and 4.90 eV for the higher-energy electrons. These values are in good agreement with those in figure 6, derived from I–V curves at nearly the same power. In addition, the nearly identical EEPFs in figure 7, obtained with and without added rare gases, is a strong confirmation that the rare gases do not alter the electron energies and concentrations in an oxygen plasma.

Deviation of the EEDFs from Maxwellian forms have been reported for other inductively-coupled processing plasmas [20, 21, 33–39]. Ar and O_2 plasmas exhibit a suppressed distribution of high-energy electrons at higher pressures (>10 mTorr) [20, 21, 33–38], while at lower pressures (<10 mTorr), different distribution shapes

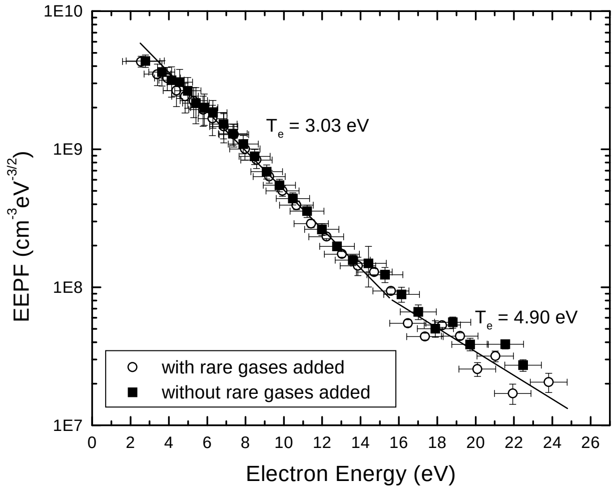

Figure 7. EEPF measured with the Langmuir probe for a 10 mTorr O_2 plasma, with and without 5% added rare gases (1% each He, Ne, Ar, Kr and Xe) at 980 W.

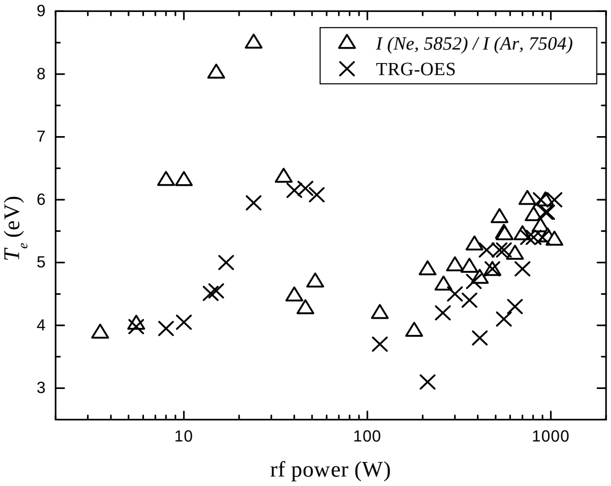

Figure 8. I(Ne, 5852)/I(Ar, 7504) against rf power in a 10 mTorr O_2 TCP with 5% trace rare gases, normalized to T_e^{OES} at 1046 W. The T_e^{OES} from figure 5 are also plotted.

have been reported. These range from distributions that can be reasonably well described by a single T_e [20, 21], to non-Maxwellian EEDFs with a low-energy peak (i.e. bi-Maxwellian) [37, 38], or with suppressed high-energy electron populations, similar to the high-pressure distributions [33, 35]. The suppression of high-energy electrons at high pressures occurs because of inelastic collisions between high-energy electrons and neutrals between ~5 and ~20 eV. Above ~20 eV (≈plasma potential), electrons are lost to the walls at all pressures. In an O_2 ICP at 10 mTorr, as the power increases the number density (mostly O_2) decreases by a factor of approximately two, due to heating. This causes the electron temperature to increase to maintain an ionization rate that balances the ion loss rate.

The behaviour of the high-energy tail of the EEDF is also reflected in the data presented in figure 8 (the ratio of the neon emission intensity at 5852 Å, I(Ne, 5852), to I(Ar, 7504) as a function of power). This $2p_1$ level of Ne is 18.26 eV above the ground state, while the energy of the $2p_1$ level of Ar is only 13.48 eV above its ground state. If the population of electrons with energies >18.26 eV increases more rapidly than the population of electrons with energies >13.48 eV, the Ne emission will increase more rapidly than the Ar emission. Therefore the Ne-to-Ar emission ratio is a qualitative indicator of the relative population of high-energy electrons. This ratio approximately tracks T_e^{OES}, especially at higher powers, and therefore confirms the behaviour of T_e^{OES} in figure 5.

The consistent evidence for bi-Maxwellian-like EEDFs in oxygen ICPs is in contrast to the equally consistent evidence in Cl_2 plasmas for Maxwellian EEDFs at pressures <5 mTorr ($T_e^{OES} = T_e^{LP}$, linear EEPF plots and very weak Ne emission), and suppressed high-energy (10–20 eV) distributions at pressures >5 mTorr ($T_e^{OES} < T_e^{LP}$, downward curving EEPF plots and very weak Ne emission) that are found in the same reactor [25].

The variation of electron temperature in the dim (capacitive) mode is also shown in figure 5. T_e^{OES} is ~4.0 eV at very low power (~7 W) and increases to ~6.1 eV at ~45 W. T_e^{LP}, however, decreases from ~3.6 eV at ~10 W to ~3.0 eV at ~45 W. The nearly equal values for T_e^{OES} and T_e^{LP} at the lower E-mode powers signify a more Maxwellian-like EEDF, as ohmic heating in the bulk of the discharge is believed to be more important than stochastic heating in the sheath regions [40]. As the rf power is increased from ~7 to 45 W, T_e^{OES} becomes increasingly larger than T_e^{LP}, as stochastic heating by electron collisions with the sheath dominates the heating in the low-field bulk regions [40–43]. Under these conditions, only high-energy electrons reach the intense electric field areas, while the low-energy electrons are trapped by the ambipolar field and equilibrate to a much lower temperature. This effect creates a bi-Maxwellian EEDF for the majority of the power range in the E-mode. Similar transitions from a Druyvesteyn distribution at very low power to a bi-Maxwellian distribution at higher powers were reported by Lieberman and Godyak [40] in a capacitively-coupled Ar plasma.

As power is abruptly increased from ~45 W to 100 W (the transition from dim (E) to bright (H) mode), T_e^{OES} decreases from ~6.1 to ~3.5 eV, an inverse dependence also observed in TCP Cl_2 plasmas [25]. T_e^{LP} also decreases with an increase in the rf power from ~3.0 eV at ~45 W to 2.7 eV at 100 W. This transition from capacitive to inductive coupling is an abrupt function of power [44], so the abrupt change observed in the EEDF is expected. Although the EEDF remains bi-Maxwellian in the transition from the E- to H-mode, it tends towards a more Maxwellian form as the difference between the two 'temperatures' measured by the two techniques decreases from ~3.0 at ~45 W to 0.8 eV at ~120 W.

The electron temperatures characteristic of the high-energy portion of the EEDF are higher than those recently measured in chlorine plasmas [23–30]. These high-energy electrons are not only important for sustaining the ionization and dissociation processes in the plasma, they are also those that are able to overcome the retarding fields and impinge on the upper sidewalls of high aspect ratio features. This causes differential charging of these high aspect ratio features and can lead to electrical damage and some etching profile anomalies. In general, higher electron temperatures exacerbate these problems, hence some advantage may be gained by operating oxygen plasmas at lower powers, subject to trade-offs in etching rates. High electron temperatures will also increase the total emission of UV light in the plasma, since the levels responsible for these emissions are at high energies. Consequently, any damaging effects induced by UV light, such as in high-density plasma deposition of SiO_2 would also be reduced by operating the plasma at lower powers and therefore at a lower electron temperature and density.

3.3. Absolute species densities

3.3.1. Excitation of the emitting species. Oxygen atoms are formed in an O_2 plasma mainly by electron impact dissociation

$$O_2 + e^- \rightarrow O + O + e^- \qquad (2)$$

or by dissociative attachment

$$O_2 + e^- \rightarrow O + O^-. \qquad (3)$$

Electron impact excitation of ground-state molecular and atomic oxygen leading to emission at 8446 Å occurs by two mechanisms, direct excitation

$$O + e^- \rightarrow O^* + e^- \qquad (4)$$

and dissociative excitation

$$O_2 + e^- \rightarrow O^* + O + e^- \qquad (5)$$

where O^* refers to the $O(3p\,^3P)$ state which emits at 8446 Å. As the power decreases, reaction (5) eventually dominates over reaction (4). This effect is obvious from the presence of a non-zero y-intercept (figure 2) in the limit of zero TCP power, where $n_O = 0$.

Walkup *et al* [9] have shown that reaction (5) leads to a Doppler-broadened emission lineshape, due to the ~1 eV spread in the velocities of the O^* produced, and because O^* spontaneous emission is faster than thermalization. We could not observe such Doppler broadening due to the limiting spectral resolution. They also reported that in an oxygen plasma that is more than 5% dissociated, reaction (4) dominates for the 8446 Å emission. Both routes (reactions (4) and (5)) were taken into account for the analysis of the 8446 Å emission line.

The $O(3p\,^3P)$ emitting species can also be produced by electron impact of metastable species:

$$O_m + e^- \rightarrow O^* + e^- \qquad (6)$$

$$O_2(a^1\Delta_g) + e^- \rightarrow O^* + O + e^- \qquad (7)$$

where O_m is either the $O(^1D)$ or $O(^1S)$ metastable (see the energy level diagram in figure 9). O_m and $O_2(a^1\Delta_g)$ are generated by

$$O_2 + e^- \rightarrow O_m + O + e^- \qquad (8)$$

$$O + e^- \rightarrow O_m + e^- \qquad (9)$$

$$O_2 + e^- \rightarrow O_2(a^1\Delta_g) + e^- \qquad (10)$$

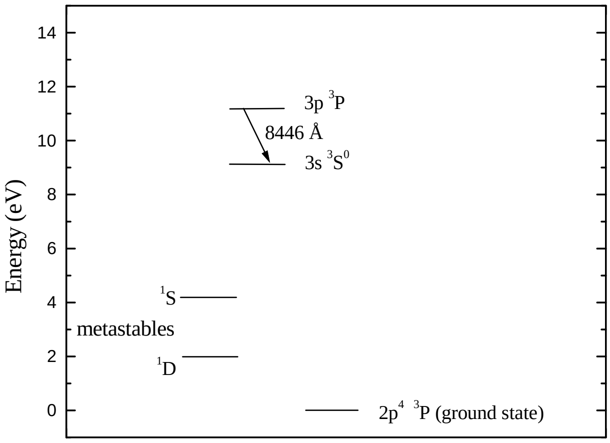

Figure 9. Energy level diagram for atomic oxygen showing optical emission at 8446 Å due to the electronic transition $3p\,^3P \rightarrow 3s\,^3S^o$.

$$O_2 + O(^1D) \rightarrow O_2(a^1\Delta_g) + O. \qquad (11)$$

As will be shown below, $O(^1D)$ and $O(^1S)$ most likely account for the small, but not negligible, fractions of the observed emission at 8446 Å at the higher powers. The contribution from $O_2(a^1\Delta_g)$ was found to be negligible, as was the formation of the O-metastables from $O_2(a^1\Delta_g)$ [45], and as such $O_2(a^1\Delta_g)$ will be ignored.

The optical emission intensity $I(k, \lambda_{ij})$ at wavelength λ_{ij}, excited by electron impact with species k is given by [23, 25, 46]:

$$\begin{aligned} I(k, \lambda_{ij}) &= 4\pi\alpha(\lambda_{ij})Q_i b_{ij} n_e n_k \int_{v_{th}}^{\infty} \sigma_{k,i}(v) v^3 f_e(v)\,dv \\ &= \alpha(\lambda_{ij})Q_i b_{ij} K_{k,i}(T_e) n_e n_k = a_k n_k \end{aligned} \qquad (12)$$

where n_k is the density of the species (ground or metastable state) in state k that undergo electron impact excitation to yield the excited state i, that fluoresces to state j; n_e is the electron density; $\alpha(\lambda_{ij})$ is the overall light collection efficiency and spectrometer and detector sensitivity at the given wavelength; $\sigma_{k,i}$ is the effective cross section from state k to state i with threshold electron speed v_{th}, including electron impact excitation from state k to states above i that optically cascade to state i rapidly; and Q_{ij} is the quantum yield for optical emission from i to j, and can be assumed to be unity because the radiative lifetimes of the emitting states are much shorter than the time constant for electronic quenching at these low pressures. The branching ratio b_{ij} is the ratio of the intensity for the i to j transition to the sum of the intensities of all possible transitions from the level i to any lower level. For the O 8446 Å and Ar 7504 Å emissions, $b_{ij} = 1.0$. A Maxwellian electron distribution for electron energies from ~2 to 17 eV, defined by T_e^{OES} in figure 5, is assumed in using equation (12) to determine these coefficients, as well as the rate coefficient, $K_{k,i}(T_e)$.

The overall proportionality coefficient a_k on the right-hand side of (12) is represented by the coefficients a_m in the expression for O-atom emission at 8446 Å.

$$\begin{aligned} I(\mathrm{O}, 8446) = {} & a_O n_O + a_{O_2} n_{O_2} + a_{O(^1D)} n_{O(^1D)} \\ & + a_{O(^1S)} n_{O(^1S)}. \end{aligned} \qquad (13)$$

Similarly, the argon emission intensity at 7504 Å is

$$I(\mathrm{Ar}, 7504) = cn_{Ar} \tag{14}$$

where c represents a_k in (12) and n_{Ar} is the argon density determined from the input flow rate, the plasma gas temperature, T_g, and the pressure.

Excluding trace species, the oxygen mass balance is

$$n^o_{O_2} = \left(n_{O_2} + \frac{1}{2}(n_O + n_{O(^1D)} + n_{O(^1S)})\right)\left(\frac{T_g}{T_w}\right) \tag{15}$$

where $n^o_{O_2}$ is the concentration of O_2 when the plasma is off and T_g is the gas temperature which is assumed to vary linearly with rf power from $T_w = 300$ K (the reactor-wall temperature) at 0 W to 500 K at 1046 W. Equation (15) is consistent with the unchanging pressure when the plasma is turned on.

The steady-state solution for the number density of metastables that are generated through reactions (7)–(10) is given by

$$n_{O_m} = \frac{K_{m,O}n_On_e + K_{m,O_2}n_{O_2}n_e}{K_{d,i} + K_{qe}n_e + K_{qO}n_O + K_{qO_2}n_{O_2}} \tag{16}$$

where n_{O_m} represents the density O(^{1}D) and O(^{1}S) of metastables, and K_{qe}, K_{qO_2} and K_{qO} are the quenching rate constants of the metastables by electrons, O_2 molecules and O atoms, respectively. $K_{d,i}$ is the first-order diffusivity rate constant [47] for plasma species i (O, O(^{1}D) and O(^{1}S)):

$$K_{d,i} = 2D_{eff}\gamma_i/l^2_{eff} \tag{17}$$

where D_{eff} is the effective diffusion constant for each of O, O(^{1}D) and O(^{1}S) [48], l_{eff} is the effective reactor dimension, which is taken as the reactor volume to surface area ratio (3.6 cm), and γ_i is the probability that each of O, O(^{1}D) and O(^{1}S) will be lost at the walls (assumed to be unity for the two metastables). The effective diffusion coefficient, D_{eff}, (cm^2 s^{-1}) of O and each of the three metastables (A) in the predominantly O_2 background gas was estimated from

$$\frac{1}{D_{eff}} = \frac{1}{D_{(A,O_2)}} + \frac{1}{D_{Kn,A}} \tag{18}$$

where

$$D_{(A,B)} = \left(\frac{T_g}{273}\right)^{5/6}\left(\frac{N_O}{n_{O_2}}\right)\left(\frac{2.02}{\sqrt{\mu_{(A,B)}}\sqrt[3]{C6_{eff}}}\right) \tag{19}$$

$$D_{Kn,A} = \frac{v_A l_{eff}}{3} \tag{20}$$

N_O is 2.69×10^{19} cm^{-3}, $\mu_{(A,O_2)}$ is the reduced mass of A and O_2 (in amu), $C6_{eff}$ is the effective long-range interaction (in eV Å^6), and v_A is the mean thermal velocity of A [49]. $C6_{eff} = 22.56, 23.01$ and 40.97 for O, O(^{1}S) and $O_2(a^1\Delta_g)$, respectively [48].

As mentioned above and shown below $O_2(a^1\Delta_g)$ does not contribute a significant amount to the 8446 Å emission and can therefore be ignored. In addition, it is shown below that most of the O(^{1}D) and O(^{1}S) are formed by electron impact dissociation of O_2. To eliminate some of the errors associated with determining the contribution of O(^{1}D) and O(^{1}S) to the emission intensity, their number densities are computed relative to that of ground-state O, using (16), and its analogue for n_O:

$$n_{O_m} = n_O\frac{(K_8 + K_9 n_O/n_{O_2})K_{d,O}}{(2K_2 + K_8)(K_{d,m} + K_{qO_2}n_{O_2})} \tag{21}$$

where K_2 is the rate coefficient for dissociation of O_2 by electrons (essentially reaction (2), since dissociative attachment, reaction (3), is much slower) [45], K_8 is the electron impact rate coefficient for reaction (8), $K_{d,O}$ is the first-order rate coefficient for the loss of O by diffusion to and recombination at the walls and $K_{d,m}$ is the first-order rate coefficients for the loss of O metastables by diffusion to and quenching at the walls.

Initially, metastables are ignored and equations (12)–(15) are used to derive an expression for the absolute ground-state O-atom density, n_O

$$n_O = \left(\frac{T_w}{T_g}\right) \times \left(\frac{n_{Ar}K_{Ar}[I(\mathrm{O}, 8446)/I(\mathrm{Ar}, 7504)] - K_{O_2}n^o_{O_2}}{K_O}\right). \tag{22}$$

The initial values of n_O and n_{O_2} (from equation (15)) are used to compute the O-metastable densities using (21). These metastable densities are then used to re-calculate n_O and n_{O_2}. This iterative process is repeated until the densities of each of the neutral species converge. The cross sections and rate constants used in the model, and an assessment of the relative importance of the various channels for excitation of optical emission, are now presented.

3.3.2. Cross sections and rate constants.

Ar electron impact excitation cross section data by Chilton *et al* [31] were used for actinometry and to estimate relative electron densities. These cross sections include contributions from cascading from higher levels under the optically thin conditions for each of the rare gases. The rate coefficients computed from these cross sections are presented as a function of T_e in figure 10(a). Other cross sections for TRG–OES computations of T_e^{OES} are reviewed elsewhere [49].

Cross sections for electron impact excitation of O were reviewed by Laher and Gilmore [50], while those for O_2 were compiled by Itikawa *et al* [51]. Unfortunately, no measurements have been published of the cross section for excitation of the 8446 Å emission that includes cascading transitions from higher states that are also populated by electron impact. A lower limit for the cross sections for excitation of emission at 8446 Å can be obtained from the cross section for direct excitation of the 3p ^{3}P state. These data were used to compute the rate coefficients as a function of T_e, presented in figure 10(a). The rate coefficients divided by those for excitation of the Ar 7504 Å emission are included in figure 10(b).

To compute the total electron impact excitation rate for the 3p ^{3}P state, cascade transitions from higher levels of the triplet manifold—mainly ns ($n \geqslant 4$), np ($n \geqslant 4$), nd ($n \geqslant 3$) and 3s′—must also be considered [9, 52, 53]. All of these levels can undergo transitions to either the 3p ^{3}P

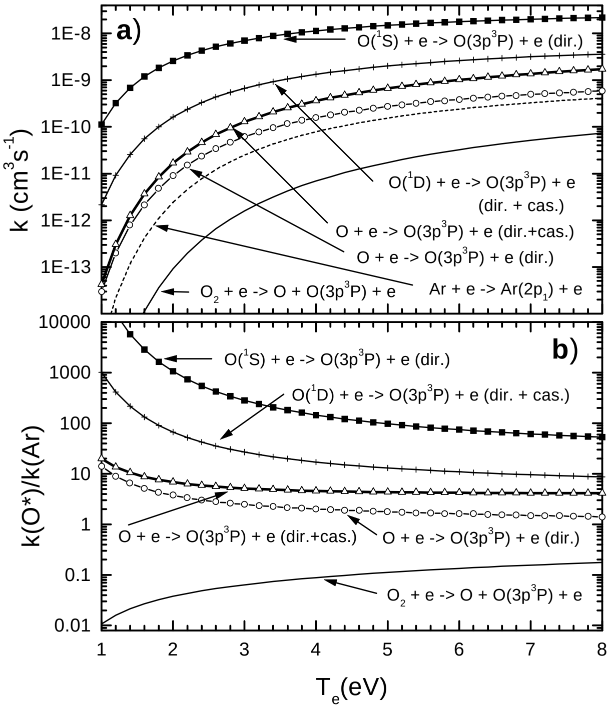

Figure 10. (a) Rate coefficients for excitation of O(3p ^{3}P), emitting at 8446 Å and for Ar(2p$_1$), emitting at 7504 Å and (b) rate constants for O(3p ^{3}P) divided by that for Ar(2p$_1$).

level, accompanied by the emission of a visible–near infrared photon, or to the ground state, resulting in emission of a vacuum-UV photon. In the optically thin limit of extremely low O-atom concentrations, these vacuum-UV transitions dominate the lower energy transitions, with Einstein *A*-factors that are typically an order of magnitude higher, hence cascading should contribute less than direct excitation of the 3p ^{3}P level. At the O-atom number densities in the present study, however, cascading is further complicated at higher powers by trapping of the vacuum-UV radiation from excited states above the 3p ^{3}P level under optically dense conditions [52–55]†. Under these circumstances, the vacuum-UV photons cannot escape the plasma and these higher levels are repeatedly excited until they decay to the 3p ^{3}P level. Therefore, the total cross section for excitation of the 3p ^{3}P level and emission at 8446 Å is nearly equal to the sum of the cross sections for direct excitation of the 3p ^{3}P level and all of the cascade levels above it. The rate constant computed from the sum of these cross sections (from Laher and Gilmore's compilation [50]) is presented in figure 10(a), and relative to Ar emission rate coefficients in figure 10(b). These latter values are used to compute the O-atom densities in this study. As can be seen from figure 10(b), the total excitation rate that includes cascade contributions to O-atom emission at 8446 Å is about three times the direct excitation rate.

Cross sections that include cascade contributions under optically thin conditions have been reported for excitation of the O 8446 Å emission by dissociative excitation of O$_2$ (reaction (5)) [56]. Because the O-atoms generated by dissociative excitation are created with large amounts of translational energy, trapping of the Doppler-broadened radiation is much less important for reaction (5) than for reaction (4). Consequently, radiation trapping was ignored for reaction (5). In the limit of zero discharge power, all of the O 8446 Å emission originates due to dissociative excitation. To force the computed emission ratio to agree with the observed ratio of 8.4 at zero power and $T_e = 4.0$ eV (see figures 1 and 4), the cross sections of Schulman *et al* [56] for reaction (5) were multiplied by 1.25. This factor is within the reported uncertainties in the O and Ar data. The cross section for reaction (5), adjusted in this manner, was used to compute rate coefficients (figure 10(a)), and the rate coefficients ratios relative to Ar emission (figure 10(b)).

The electron impact cross sections reviewed by Laher and Gilmore [50] were used for excitation of O to its ^{1}D and ^{1}S metastable levels (reaction (10)). Unfortunately, there is some ambiguity in the literature on the rate of electron impact dissociation of O$_2$ and the branching ratio between channels that generate the two ground-state O-atoms and those that form O + O(^{1}D) (i.e. reaction (8)). Cosby [57] reported the total cross sections for the production of all of the states of O. In addition, Cosby measured the translational energy released into the recoiling O-atoms. From the Franck–Condon principle, these energy spectra infer similar partitioning into the O + O and O + O(^{1}D) channels at electron energies of ∼30 eV. Below ∼20 eV the so-called 6 eV states (c $^1\Sigma_u^-$, A $^3\Sigma_u^+$, and C$^3\Delta_u$), which adiabatically dissociate into only ground-state O-atoms, are also excited. Taking the 6 eV state cross sections recommended by Itikawa *et al* [51] to be correct between the threshold (∼6 eV) and its peak of 1.5×10^{-17} cm^2 at 10 eV, assuming the cross section then increases linearly to 2.2×10^{-17} cm^2 at 13.5 eV (the lowest energy measured by Cosby [57]), using Cosby's cross sections at 13.5 eV and higher energies, assuming a 100% yield of ground-state O atoms below 18 eV and equal yields of O + O and O + O(^{1}D) above 18 eV, we have generated cross sections for reactions (2) and (8), and the rate constant expressions $K_2 = 8.08 \times 10^{-9}\exp(-7.32/T_e)$ and $K_8(^1\mathrm{D}) = 9.37 \times 10^{-9}\exp(-10.03/T_e)$ cm^3 s^{-1}.

At the highest power, $T_e = 6$ eV and the rate constant for the production of O(^{1}D) by reaction (8) ($\sim 1.8 \times 10^{-9}$ cm^2 s^{-1}) is nearly equal to that calculated for reaction (9) (3.0×10^{-9} cm^2 s^{-1}), using cross sections

---

† The absorption coefficient, k_0, at the centre of a Doppler-broadened line is given by [54]

$$k_0 = \frac{2}{\Delta\nu_D}\sqrt{\frac{\ln 2}{\pi}}\frac{\pi e^2}{m_e c}Nf$$

where N is the number density of absorbing species (i.e. ground-state O-atoms), f is the oscillator strength (e.g. 0.047 for the $^3\mathrm{P} \rightarrow {}^3\mathrm{D}^o$ 988.777 Å line [55]) and $\Delta\nu_D$ is the doppler width

$$\Delta\nu_D = \frac{2\sqrt{2R\ln 2}}{c}\nu_0\sqrt{\frac{T_g}{M}}$$

where M is the mass of O and ν_0 is the frequency of the 988.777 Å transition (3.031×10^{15} s^{-1}). For $T_g = 500$ K, $k_0 N = 1.36 \times 10^{-13} N$ (cm^2). For $N = 2 \times 10^{13}$ cm^{-3}, $1/e$ of the light at ν_0 will be absorbed in $l = 1/k_0 N = 0.37$ cm. If light were re-emitted each time at ν_0, then the distance before emission of a near-infra-red–visible photon (7990 Å in this example) accompanying a transition to the 3p ^{3}P level would be $\approx l\sqrt{A_{988}/A_{7990}} = 0.37\sqrt{2.3/0.290} = 1.0$ cm, where A_{988} and A_{7990} are Einstein *A*-factors [55]. Since light will be re-emitted over the Doppler width, assuming a uniform temperature, the distance before emission of a 8446 Å photon will be roughly twice this distance, but still much smaller than the plasma dimensions (∼10 cm).

from Laher and Gilmore [50]. Consequently, reaction (8) is the main source for the production of O(^{1}D) at all powers, since $n_O/n_{O_2} < 0.1$ at 1000 W (see below).

No experimental cross sectional data are available for the atomic metastable excitation to O(3p ^{3}P) (reaction (6)). However, *ab initio* rate constants were computed by Gordillo-Vazquez and Kunc [58] for this reaction, $K_{6,direct}$ (^{1}D) $= 6.472\times10^{-9}\ T_e^{-0.16701}\ \exp(-8.884/T_e)$ and $K_{6,direct}$ (^{1}S) $= 8.22\times10^{-8}\ T_e^{-0.23905}\ \exp(-6.591/T_e)$, where the subscript *direct* indicates that no cascading from higher levels is included. To estimate the accuracy of this rate coefficient for the direct reaction, the rate coefficients computed by Gordillo-Vazquez and Kunc [58] for reactions (4) and (9), and the reaction forming O(3p ^{5}P) from ground-state O were compared with those computed from measured cross sections given for these reactions in the review by Laher and Gilmore [50]. Throughout the range of electron temperature of interest here (2–6 eV), the rate coefficients computed by Gordillo-Vazquez and Kunc for reaction (9) are in excellent agreement with the measured values, while those for the other two reactions exceed the measured values by factors of three and six (for reaction (3)). Consequently, $K_{6,direct}$ could be high by similar factors, but it is probably not lower than the measured values. To account for cascading in an optically thick regime, $K_{6,direct}$ for O(^{1}D) was multiplied by a factor of 2.4 (independent of T_e), the same value as that computed for the cascading contribution to excitation of the 3p ^{3}P state from the ground state. For O(^{1}S), the direct excitation rate constant for the 3p ^{3}P state is so much larger than any other rate constant computed by Gordillo-Vazquez and Kunc for excitation of the ^{1}S state that we ignored any added contribution from the cascade transitions from higher excited states. Therefore, we used $K_6(^1\mathrm{D}) = 1.55\times10^{-8}\ T_e^{-0.16701}\ \exp(-8.884/T_e)$ and $K_6(^1\mathrm{S}) = 8.22\times10^{-8}\ T_e^{-0.23905}\ \exp(-6.591/T_e)$.

Loss of O(^{1}D) is primarily due to diffusion to and loss at the walls ($K_d \sim 2500$ s^{-1} for $\gamma = 1$, and $T_g = 500$ K) and quenching by O$_2$ ($K_{qO_2} = 3.7\times10^{-11}$ cm^3 s^{-1}) [59] and by electrons. The total quenching rate by electrons is the sum of rates of excitation of all of the states above†, as well as ionization. To estimate the total quenching rate constant by electrons, we included direct excitation to the ^{1}S, 3s ^{5}S^o, and 3s ^{3}S^o states, direct plus cascade (optically thick) excitation to the 3p ^{3}P state (i.e. $K_6(^1\mathrm{D})$) [59] and ionization ($k_{iz} = 9.0\times10^{-9}\ T_e^{0.7}\ \exp(-11.6/T_e)$ cm^2 s^{-1}) [19]. For $n_e = 3.7\times10^{10}$ cm^{-3}, $n_{O_2} = 1.8\times10^{14}$ cm^{-3} and $T_e = 6$ eV, $K_{qe} = 1.5\times10^{-8}$, quenching by O$_2$ and electrons occur at rates of 6620 s^{-1} and 560 s^{-1}, respectively.

Khvorostovskaya and Yankovskii [60] reported estimated rate constants for dissociative excitation from O$_2$ to O + O(^{1}S) (reaction (8)). An unpublished peak cross section of $<2\times10^{-17}$ cm^2 was measured by Zipf, as reported by Vialle *et al* [61]. This peak cross section falls in between the value of $\sim5\times10^{-17}$ cm^2 for the production of O + O(^{1}D) and 4×10^{-18} cm^2 for O + O(3p ^{3}P), as might be expected. Apparently, no other measurements or calculations have been reported for the production of O + O(^{1}S) from reaction (8). At $T_e = 6$ eV, a reasonable assumption for its rate coefficient would be between that for production of O + O(^{1}D) (1.8×10^{-9}) and O + O(3p ^{3}P) (3.2×10^{-11}), i.e. $\sim3\times10^{-10}$ cm^2 s^{-1}, and by equivalent interpolation $\sim1\times10^{-10}$ cm^2 s^{-1} at $T_e = 4.5$ eV. These rate constants are about an order of magnitude larger than those reported by Kvorostovskaya and Yankovskii [60]. The larger rate constants estimated by interpolation were used in this study. They are about the same as those for the production of O(^{1}S) from O. Given that $n_O/n_{O_2} < 0.1$ at 1000 W, reaction (8) therefore dominates over reaction (9) for O(^{1}S) production. The loss rate of O(^{1}S) by diffusion to the walls is $K_d \sim 2500$ s^{-1}. The quenching rate constants by O$_2$ is 7×10^{-13} cm^2 s^{-1} [62] and by electrons is $\sim4\times10^{-8}$ cm^3 s^{-1} (see the previous paragraph). Thus, for $n_e = 3.7\times10^{10}$ cm^{-3}, $n_{O_2} = 1.8\times10^{14}$ cm^{-3} and $T_e = 6$ eV, the loss of O(^{1}S) from quenching by electrons (1480 s^{-1}) is a factor of $\sim$1.7 smaller than diffusion-controlled quenching at the walls, while quenching by O$_2$ (126 s^{-1}) is much less.

The cross sections recommended by Itikawa *et al* [51] were used for electron impact excitation of O$_2$ to the a$^1\Delta_g$ state (reaction (10)). For n_e of 3.7×10^{10} cm^{-3} and $n_{O(^1D)}$ of 5.2×10^{11} cm^{-3} and T_e and T_g of 6.0 eV and 500 K respectively, the production rate of O$_2$ (a$^1\Delta_g$) by reaction (10) ($K_{10} = 9.4\times10^{-10}$ cm^3 s^{-1}) [51] is about twice that by reaction (11) ($K_{11} = 3.7\times10^{-11}$ cm^2 s^{-1}) [59]. Therefore, reaction (10) is the dominant route for the production of O$_2$(a$^1\Delta_g$).

The quenching rate constants of O$_2$ (a$^1\Delta_g$) by molecular and atomic oxygen are both very small ($K_{qO_2} = 2.3\times10^{-18}$ cm^2 s^{-1} and $K_{qO} = 2.0\times10^{-16}$ cm^3 s^{-1}) [59]; consequently, it is lost mainly by diffusion to the walls ($K_d = 2.1\times10^3$ s^{-1}). At $T_e = 6$ eV and $T_g = 500$ K (1046 W), using the above production and quenching rate constants of O$_2$ (a$^1\Delta_g$), a value of 5×10^{-3} is estimated for $n_{O_2(a^1\Delta_g)}/n_{O_2}$ from equation (15). Neither the experimental nor the calculated data are available for the dissociative excitation from O$_2$(a$^1\Delta_g$) to O(3p ^{3}P) (reaction (7)). Even when likely overestimates of the rate constant on the order of $\sim10^{-8}$ cm^{-3} s^{-1} are used in this calculation, the contribution of this route to the 8446 Å emission line is negligible, and therefore was ignored.

3.3.3. Resulting absolute number densities. The absolute densities of O and O$_2$ and of the metastables species (O(^{1}D) and O(^{1}S)), determined using the iterative process described above, are presented in figures 11 and 12, respectively, as function of the applied rf power. The ground-state atomic oxygen density increases with increasing rf power from $\sim6.6\times10^{12}$ cm^{-3} ($\sim$1% dissociation) at 400 W to 1.1×10^{13} cm^{-3} ($\sim$2% dissociation) for a maximum power density of 1046 W (5.7 W cm^{-2}). At the highest power density of 5.7 W cm^{-2} (1046 W), the O(^{1}D) and O(^{1}S) densities

---

† The total excitation rate coefficient was estimated from the sum of the rate constants for electron impact excitation from O(^{1}D) to ^{1}S, 3s ^{5}S^o, 3s ^{3}S^o, 3p ^{5}P and 3p ^{3}P. The direct excitation rate constants for excitation to the 3p ^{5}P and 3p ^{3}P states were multiplied by 2.4 (the enhancement factor for cascading in the optically thick limit—see text above). By including the cascade transitions for an optically thick medium, excitation to all excited states above 3p ^{3,5}P is included. The total excitation rate coefficient for the ^{1}S state is treated in an analogous manner. As in Lee *et al* [19] for O(^{1}D), we estimate $k_{iz} = 9.0\times10^{-9}\ T_e^{0.7}\ \exp(-9.4/T_e)$ cm^2 s^{-1} for ionization of O(^{1}S) by using the same pre-exponential factors as for ionization of ground-state O and an activation energy of 9.4 eV (the difference in the first ionization potential of O (13.6 eV) and the energy of O(^{1}S)), instead of 13.6 eV.

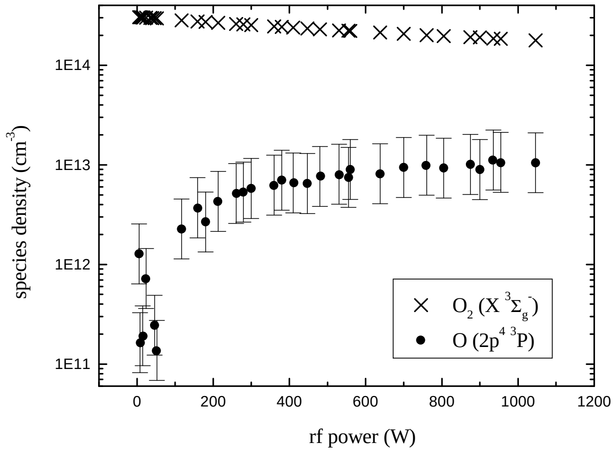

Figure 11. The absolute densities of ground-state O and O_2 against rf power in a 10 mTorr O_2 TCP with 5% of the trace rare gas mixture.

were 5 and 1% of the ground-state O density, respectively, and O, O(^{1}D), O(^{1}S) and O_2 are responsible for 56, 4, 16 and 24% of the total O emission intensity at 8446 Å. Based mostly on the uncertainties in the cross section data, the O-atom ground-state densities are probably accurate to within a factor of two†. The error bars on the O-atom measurements in figure 11 reflect this overall approximate uncertainty.

The degree of dissociation found in the present study is much less than that predicted in the modelling studies by Lee *et al* [19] for a 10 mTorr O_2 plasma at comparable power densities. In that study, heterogeneous recombination of O-atoms was not considered in most of their predictions. When wall recombination was included with a recombination coefficient of 0.1, much lower degrees of dissociation were predicted.

Lower degrees of dissociation than those predicted by Lee *et al* [19] were also measured by Granier *et al* [15, 16] in an oxygen high-density helicon plasma (e.g. 10% at 500 W). They attribute this small amount of dissociation at high plasma density to a very high rate of recombination of O-atoms on the walls of the chamber. High wall recombination rates and low degrees of dissociation were also reported by Matsushita *et al* [63] in an oxygen helicon plasma.

We can estimate the degree of dissociation from the zero-D model steady-state expression:

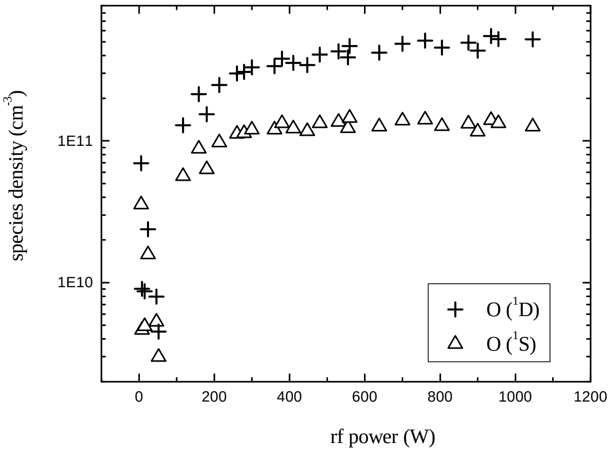

Figure 12. O(^{1}D) and O(^{1}S) number densities against rf power in a 10 mTorr O_2 TCP with 5% of the trace rare gas mixture, computed from the model and using the measured O and O_2 number densities from the optical emission measurements.

$$n_O = \frac{[2K_2 + K_8(^1\mathrm{D})]n_e n^o_{O_2}}{K_{d,O} + K_{iz} n_e}\left(\frac{T_w}{T_g}\right) \qquad (23)$$

where K_{iz} is the ionization rate coefficient for O ($K_{iz} = 9 \times 10^{-9} T_e^{0.7} \exp(-13.6/T_e)$ cm^{-3} s^{-1}) [19]. If we assume that the negative ion density is much less than the positive ion density so that $n_e = n_i^+ = 3.7 \times 10^{10}$ cm^{-3}, and further assume that $T_g = 500$ K and $\gamma_O = 0.4$ on the mostly stainless-steel surfaces [64], then $n_O = 3.5 \times 10^{13}$ cm^3 from (20). This estimate is close to (about three times higher than) that derived from the optical emission measurements—reasonable agreement given the assumptions in measuring and computing n_O. (A lower electron density due the presence of negative ions would move the computed value closer to the observed O-atom density.) Therefore, the low degrees of O_2 dissociation measured in this study are reasonable.

The etching rates of low-*k* organic films would be expected to increase with increasing O-atom density until ion-flux-limited conditions are obtained. This regime may not be reached at the relatively low O-atom densities obtainable with a system containing internal surfaces that exhibit a high recombination rate for O, regenerating O_2. Presumably, higher O-atom concentrations would be present in systems with anodized-aluminum-, quartz- or SiO_2-coated walls. This may not necessarily be desirable, since O-atoms will also react spontaneously with organic materials, leading to undercutting and the need for the addition of sidewall-inhibitor species to the plasma. The control of the degree of O_2 dissociation by the choice of wall materials may thus offer a method to optimize the O-atom concentration, and therefore balance the etching rate and the degree of undercutting with a minimum of added sidewall inhibitor. In addition, the formation of passivating layers on the chamber walls, from additives and from etching products, will be likely to decrease the O-atom recombination rate and lead to an increase in the O-atom densities.

---

† As mentioned above, we assume that the entire EEDF is described by a T_e equal to T_e^{OES}. Most processes that are important for measuring the O-atom densities by actinometry, and for computing the dissociation of O_2, occur at high electron energies and therefore are induced by the same part of the EEDF that is measured by TRG–OES. Consequently, T_e^{OES} is the better temperature to use. The only exception is excitation of O(^{1}D) and O(^{1}S). For these levels, an EEDF described by a combination of T_e^{OES} and T_e^{LP} (e.g. 5 and 3 eV, respectively, at 700 W) would perhaps be better. The rate constant for excitation for O(^{1}S) and (^{1}D) decreases by factors of two and three, respectively, when T_e decreases from 5 to 3 eV. The optimum, effective electron temperature would be somewhere in between, so perhaps we are overestimating the excitation rates of O(^{1}S) and O(^{1}D) by factors of ~1.5 and ~2. If we decrease these excitation rates by these amounts, the O ground-state density in figure 11 would increase by ~30%. Because other factors are likely to contribute more uncertainty (the rate constants for O(^{1}D) and O(^{1}S) are probably uncertain within a factor of two, for example), the Maxwellian T_e assumption is reasonable.

4. Conclusions

Oxygen TCPs were investigated by optical emission and Langmuir probe analysis. The absolute number densities of ground-state oxygen atoms were derived from O-atom optical emission at 8446 Å, combined with Ar emission actinometry and modelling. The roles of ground-state O and O_2 and metastable O(^{1}D), O(^{1}S) and $O_2(a^1\Delta_g)$ in exciting the O emission were evaluated. All but $O_2(a^1\Delta_g)$ were found to contribute significantly, with ground-state O being dominant at high powers. In this mostly stainless-steel and quartz reactor, O_2 dissociation is minimal ($\sim$2%), even at the maximum inductively-coupled power of 1046 W (5.7 W cm^{-2}), in good qualitative agreement with global model predictions. At this high power, O(^{1}D) and O(^{1}S) densities were 5 and 1% of the ground-state O density, respectively. In the capacitively-coupled, E-mode ($<$100 W), the gas is expected to be primarily comprised of O_2 with ground-state O and the three metastable species having negligible concentrations.

Electron temperatures characteristic of the tail of the EEDF were measured by TRG–OES. The electron temperature increases with the applied rf power in the H-mode (100–1046 W) from 2.7 to 3.4 eV for electrons sampled by the Langmuir Probe and from $\sim$3.5 to 6.0 eV for high-energy electrons sampled by the TRG–OES technique. In the E-(capacitive) mode, below 45 W, T_e measured by TRG–OES varies directly with rf power, increasing from a $\sim$4.0 eV for negligible rf power, to $\sim$6.1 eV at 45 W. The T_e measured by TRG–OES varies inversely with the rf power, from 6.1 eV at $\sim$45 W (highest E-mode power) to $\sim$3.5 eV at $\sim$100 W (lowest H-mode power), and T_e derived from Langmuir probe measurements also varies inversely with the rf power, from $\sim$3.0 eV at $\sim$45 W to $\sim$2.6 eV at $\sim$100 W. In the H-mode, the EEDF is bi-Maxwellian throughout the rf power range investigated in this regime. In the E-mode, the EEDF changes from nearly Maxwellian (possibly Druyvesteyn) at low rf powers ($\sim$7 W) to bi-Maxwellian at the higher E-mode powers ($\sim$50 W), seemingly due to the stochastic heating of the high-energy electrons by the oscillating plasma sheath.

Acknowledgments

We thank Lowell Morgan for discussions and recommendations on electron impact dissociation mechanisms and diffusion coefficients, and Joseph Kunc for providing rate coefficients for some of the electron impact excitation reactions. This work was supported in part by NSF grant No DMR-98-15846 (for NCMF and IPH).

References

[1] Flamm D L, Donnelly V M and Ibbotson D E 1984 *VLSI Electronics Microstructure Science* ed N G Einspruch and D M Brown (Orlando, FL: Academic) ch 8
[2] Carl D A, Hess D W and Lieberman M A 1990 *J. Appl. Phys.* **68** 1859
[3] Morey I and Asthana A 1999 *Solid State Technol.* **42** 71
[4] Baklanov M R, Vanhaelemeersch S and Bender H 1999 *J. Vac. Sci. Technol.* B **17** 372
[5] Bohr M T 1995 *IEDM Tech. Digest* p 241
[6] Fujiwara N, Maruyama T, Yoneda M, Tsukamoto K and Banjo T 1994 *Japan. J. Appl. Phys.* **33** 2164
[7] Samukawa S, Nakagawa Y, Tsukada T, Ueyama H and Shinohara K 1995 *Japan. J. Appl. Phys.* **34** 6805
[8] Samukawa S 1994 *Japan. J. Appl. Phys.* **33** 2133
[9] Walkup R E, Saenger K L and Selwyn G S 1986 *J. Chem. Phys.* **84** 2668
[10] Tserepi A D and Miller T A 1995 *J. Appl. Phys.* **77** 505
[11] Collart E J H, Baggerman J A G and Visser R J 1991 *J. Appl. Phys.* **70** 5278
[12] Pagnon D, Amorim J, Nahorny J, Touzeau M and Vialle M 1995 *J. Phys. D: Appl. Phys.* **28** 1856
[13] St Behle, Georg A, Yuan Y, Engemann J and Brockhaus A 1997 *Surf. Coat. Technol.* **97** 734
[14] Booth J P, Joubert O and Pelletier J 1991 *J. Appl. Phys.* **69** 618
[15] Granier A, Nicolazo F, Vallee C, Goullet A, Turban G and Grolleau B 1997 *Plasma Sources Sci. Technol.* **6** 147
[16] Granier A, Chereau D, Henda K, Safari R and Leprince P 1994 *J. Appl. Phys.* **75** 104
[17] Lee Y H, Heidenreich J E III and Fortuno G 1989 *J. Vac. Sci. Technol.* A **7** 903
[18] Keller J H, Forster J C and Barnes M S 1993 *J. Vac. Sci. Technol.* A **11** 2487
[19] Lee C, Graves D B, Lieberman M A and Hess D W 1994 *J. Electrochem. Soc.* **141** 1546
[20] Gudmundsson J T, Kimura T and Lieberman M A 1999 *Plasma Sources Sci. Technol.* **8** 22
[21] Schwabedissen A, Benck E C and Roberts J R 1997 *Phys. Rev.* E **55** 3450
[22] Coburn J W and Chen M 1980 *J. Appl. Phys.* **51** 3134
[23] Malyshev M V and Donnelly V M 1997 *J. Vac. Sci. Technol.* A **15** 550
[24] Donnelly V M, Malyshev M V, Kornblit A, Ciampa N A, Colonell J I and Lee J T C 1998 *Japan. J. Appl. Phys.* **37** 878
[25] Malyshev M V and Donnelly V M 1999 *Phys. Rev.* E **60** 6016
Malyshev M V and Donnelly V M 1999 *J. Appl. Phys.* **87**
[26] Malyshev M V, Donnelly V M, Kornblit A and Ciampa N A 1998 *J. Appl. Phys.* **84** 137
[27] Malyshev M V, Donnelly V M and Samukawa S 1998 *J. Appl. Phys.* **84** 1222
[28] Malyshev M V, Donnelly V M, Downey S W, Colonell J I and Layadi N 1999 *J. Vac. Sci. Technol.* submitted
[29] Malyshev M V, Fuller N C M, K. Bogart H A, Donnelly V M and Herman I P 1999 *Appl. Phys. Lett.* **74** 1666
[30] Malyshev M V, Donnelly V M, Colonell J I and Samukawa S 1998 *J. Appl. Phys.* **86** 4813
[31] Chilton J E, Boffard J B, Schappe R S and Lin C C 1998 *Phys. Rev.* A **57** 267
[32] Boffard J B, Piech G R, Gehrke M F, Anderson L W and Lin C C 1999 *Phys. Rev.* A **59** 2749
[33] Seo S-H, Hong J-I and Chang H-Y 1999 *Appl. Phys. Lett.* **74** 2776
[34] Haas F A and Braithwaite N St J 1999 *Appl. Phys. Lett.* **74** 338
[35] Godyak V A, Piejak R B and Alexandrovich B M 1995 *Plasma Sources Sci. Technol.* **4** 332
[36] Hopkins M B 1995 *J. Res. Natl. Inst. Stand. Technol.* **100** 415
[37] Hori T, Kogano M, Bowden M D, Uchino K and Muraoka K 1998 *J. Appl. Phys.* **83** 1909
[38] Hori T, Bowden M D, Uchino K and Muraoka K 1996 *Appl. Phys. Lett.* **69** 3683
[39] Sato M 1999 *Japan. J. Appl. Phys.* **38** 242
[40] Lieberman M A and Godyak V A 1998 *IEEE Trans. Plasma Sci.* **26** 955
[41] Wang Z, Lichtenberg A J and Cohen R H, *Plasma Sources Sci. Technol.* **8** 151
[42] Wood B P, Lieberman M A and Lichtenberg A L 1995 *IEEE Trans. Plasma Sci.* **23** 89
[43] Wang Z, Lichtenberg A J and Cohen R H 1998 *IEEE Trans. Plasma Sci.* **26** 59
[44] Turner M A and Lieberman M A 1999 *Plasma Sources Sci. Technol.* **8** 313
[45] Eliason B and Kogelschatz U 1986 *Basic Data for Modeling of Electrical Discharges in Gases: Oxygen KLR* 86-11 C

[46] Lieberman M A and Lichtenberg A J 1994 *Principles of Plasma Discharges and Materials Processing* (New York: Wiley) p 257

[47] Lieberman M A and Lichtenberg A J 1994 *Principles of Plasma Discharges and Materials Processing* (New York: Wiley) p 291

[48] Morgan L 1999 private communication

[49] Malyshev M V 1998 *PhD Dissertation* Princeton University, Princeton NJ

[50] Laher R R and Gilmore F R 1990 *J. Phys. Chem. Ref. Data.* **19** 277

[51] Itikawa Y, Ichimura A, Onda K, Sakimoto K, Takayanagi K, Hatano Y, Hayashi M, Nishimura H and Tsurubuchi S 1989 *J. Phys. Chem. Ref. Data.* **18** 23

[52] Zipf E C and Stone E J 1971 *J. Geophys. Res.* **76** 6865

[53] Julienne P S and Davis J 1976 *J. Geophys. Res.* **81** 1397

[54] Mitchell A C G and Zemansky M W 1971 *Resonance Radiation and Excited Atoms* (Cambridge) pp 99–100

[55] Wiese W L, Smith M W and Glennon B M 1966 *Atomic Transition Probabilities, Hydrogen Through Neon (National Bureau of Standards Reference Data Series, I)* (Washington, DC: National Bureau of Standards) pp 77–82

[56] Schulman M B, Sharpton F A, Chung S, Lin C C and Anderson L W 1985 *Phys. Rev.* A **32** 2100

[57] Cosby P C 1992 *SRI International Report* Contract No F33615-85-C-2560
Cosby P C 1992 *J. Chem. Phys.* **98** 9560

[58] Gordillo-Vazquez F J and Kunc J A 1995 *Phys. Rev.* E **51** 6010
Kunc J A 1999 Private communication for higher T_es

[59] DeMore W B, Sander S P, Golden D M, Hampson R F, Kurylo M J, Howard C J, Ravishankara A R, Kolb C E and Molina M J 1997 *Chemical Kinetics and Photochemical Data for Use in Stratospheric Modeling* Jet Propulsion Laboratory publication 97-4, Evaluation No 12

[60] Khvorostovskaya L E and Yankovskii V A 1986 *Sov. J. Chem Phys.* **3** 2478

[61] Vialle M, Touzeau M, Gousset G and Ferreira C M 1991 *J. Phys. D: Appl. Phys.* **24** 301

[62] Slanger T G, Wood B J and Black G 1972 *Chem. Phys. Lett.* **17** 401

[63] Matsushita J, Sasaki K and Kadota K 1997 *Japan. J. Appl. Phys.* **36** 4747

[64] Shibata M, Nakano N and Makabe T 1996 *J. Appl. Phys.* **80** 6142